Chinese Chemical Letters 35 (2024) 109668

Contents lists available at ScienceDirect

Chinese Chemical Letters

journal homepage: www.elsevier.com/locate/cclet

# The size-switchable microspheres co-loaded with RANK siRNA and salmon calcitonin for osteoporosis therapy

Xueyan Zhang[a], Jicong Chen[a], Songren Han[a], Shiyan Dong[b], Huan Zhang[a], Yuhong Man[d], Jie Yang[a,*], Ye Bi[c,*], Lesheng Teng[a,*]

[a] School of Life Sciences, Jilin University, Changchun 130012, China
[b] Department of Radiation Oncology, The University of Texas MD Anderson Cancer Center, Houston 77030, TX, United States
[c] Practice Training Center, Changchun University of Chinese Medicine, Changchun 130117, China
[d] Department of Neurology, The Second Hospital of Jilin University, Changchun 130041, China

ARTICLE INFO

*Article history:*
Received 13 December 2023
Revised 15 February 2024
Accepted 17 February 2024
Available online 24 February 2024

*Keywords:*
Osteoporosis
RANK siRNA
Salmon calcitonin
Nanocarriers
Size-switchable microspheres

ABSTRACT

Osteoporosis is a disease of bone metabolism homeostasis imbalance with obvious bone loss, damage to bone microstructure, and increased risk of fracture. The occurrence and development of osteoporosis is related to the augmentation of active osteoclasts. Receptor activator of nuclear factor kappa B (RANK) small interfering RNA (siRNA) knockdowns the expression of RANK mRNA to inhibit the osteoclast precursors differentiate into osteoclasts as a treatment in osteoporosis. Salmon calcitonin (sCT) is a commonly used anti-osteoporotic agent that inhibits osteoclast activity and induces osteoclast apoptosis, and it also could promote the osteogenesis by osteoblasts. A cocktail therapy improves the therapeutic effect of osteoporosis between RANK siRNA and sCT. A size-switchable microsphere from micro to nano scale was developed to address the delivery barriers of biomacromolecules with poor stability and frequent administration. RANK siRNA and sCT were incorporated into the microspheres with a nanoparticle/micelle-microsphere double-layer structure to achieve sustained release when the particle size shrunk and dual protection of RANK siRNA and sCT. The size-switchable microspheres MS@(AL-NPs/ARM) had an optimal therapeutic effect and reduced the frequency of administration in glucocorticoid induced osteoporosis (GIOP) mouse model. RANK siRNA and sCT co-delivery system based on size-switchable microsphere is a promising strategy to treat osteoporosis through the controlled release of biomacromolecules.



Osteoporosis is a bone condition characterized by bone mass loss, bone microstructure defects, and significantly increased bone fragility fracture risk [1,2]. As a serious global public health problem, osteoporosis brings heavy physical, psychological and economic burden to patients. Under physiological conditions, the maintenance of bone metabolism homeostasis depends on the dynamic balance of bone reconstruction process between the osteoblast-mediated bone formation and osteoclast-mediated bone absorption [3,4]. The increase in differentiation and activity of osteoclasts is critical in terms of excessive bone resorption and disrupted bone remodeling, resulting in osteoporosis [5].

In the past 20 years, various drugs have been developed to inhibit osteoclast-mediated bone resorption, including bisphosphonates such as alendronate (AL) and risedronate [6]; estrogen, such as estradiol and estriol [7]; selective estrogen receptor modulator [8], such as raloxifene; calcitonin [3], such as salmon calcitonin and eel calcitonin, *etc.* However, these treatment methods showed obvious limitations, including poor therapeutic effects and safety issues with long-term treatment. For example, AL can only inhibit the further deterioration of osteoporosis, but cannot supplement lost bones [9]; estrogen has side effects such as breast cancer with long-term use [10]. In addition, some drugs have a single function and can only target a certain stage of osteoclast development. AL, for instance, is more effective in the early stages of osteoclast development [11]; salmon calcitonin (sCT) can more effectively inhibit the activity of mature osteoclasts and kill them at the later stage of osteoclast development [12]. Therefore, finding a suitable treatment method for osteoporosis remains an urgent need in clinical practice.

In fact, osteoclast precursors and mature cells all coexist during the maturation of osteoclasts. Therefore, the co-delivery of two drugs that inhibit different stages of osteoclast development is considered valuable. The receptor activator of nuclear factor kappa B (RANK)/RANK ligand (RANKL) signaling pathway has been con-

* Corresponding authors.
*E-mail addresses:* jieyang@jlu.edu.cn (J. Yang), biye88@outlook.com (Y. Bi), tenglesheng@jlu.edu.cn (L. Teng).

https://doi.org/10.1016/j.cclet.2024.109668
1001-8417/

firmed as a more effective therapeutic target in osteoporosis, which is involved in the transcriptional regulation of osteoclast precursors to differentiate into mature osteoclasts [13–15]. Small interfering RNA of RANK (RANK siRNA), which blocks a membrane protein of RANK expression in osteoclast precursors, inhibits osteoclast phenotypic function and osteoclast-mediated bone resorption *in vitro* [16]. Another stage of osteoporosis is associated with mature osteoclasts degrading the bone extracellular matrix, which is promptly inhibited by sCT, a 32-amino acid peptide that binds to calcitonin receptor (CTR), following the loss of the ruffled border and halting bone resorption [12,17]. RANK siRNA suppressed the transformation of osteoclast precursors into osteoclasts, while sCT inhibited osteoclast proliferation and activity. The combination of RANK siRNA and sCT may achieve an advanced therapeutic effect, as they act on different processes of bone transformation. In addition, sCT can promote bone formation by activating osteoblasts, which may also enhance the therapeutic effect of osteoporosis.

However, as the clinical application of biomacromolecule-based agents, RANK siRNA and sCT are limited by their short half-life and frequent administration [18,19]. Based on this issue, numerous researchers have developed various drug delivery systems to achieve the sustained release of biomacromolecule-based agents. Among them, biodegradable polymer microspheres are widely studied as drug carrier, capable of achieving sustained drug release in the blood circulation and reducing dosing frequency. Wang *et al*. developed an injectable drug carrier, that is, polylactic acid microsphere coated with tannic acid/polyethylene glycol-modified sCT (TA/PEG-sCT) layer-by-layer films and demonstrated that a single injection of the carrier could maintain plasma levels of PEG-sCT for an extended period *in vivo* [20]. Similarly, Li *et al*. prepared poly(lactic-*co*-glycolic acid) (PLGA) microspheres as sustained-release carriers for delivering sclerostin single-chain antibody fragments for osteoporosis treatment [21]. However, the released biomacromolecules from microspheres were naked, unstable, not target specific and had low cellular uptake [22,23]. Nanotechnology is an effective approach to deliver agents to target sites and prevent their degradation in the physiological environment of the systemic circulation [24–27]. Sun *et al*. prepared a polymer nanoparticle composed of the pH-sensitive polymer PK3, folate-PEG-PLGA and 1,2-dioleoyl-3-trimethylammonium-propane (DOTAP)/siRNA core for delivering siRNA targeting inflammatory joints. The polymeric nanoparticles demonstrated inflammation-targeting activity and potent therapeutic effects in a rat model of adjuvant-induced arthritis [28]. Omidi *et al*. encapsulated vascular endothelial growth factor (VEGF) in soybean L-$\alpha$-phosphatidyl ethanolamine and L-$\alpha$-phosphatidyl choline anhydrous reverse micelle (ARM) nanoparticles, and then encapsulated them into PLGA microspheres by microfluidic method to preserve the activity of VEGF and achieve sustained release [29].

Considering that delivery therapeutic entities of biomacromolecule-based agents with high stability, longer half-life, tissues-targeted manner and low administration frequency is a major challenge for the scientific community. Therefore, for anti-osteoporotic therapy, it is crucial to design a carrier that continuously co-delivers RANK siRNA and sCT to the lesion site. In this study, we utilized the advantages of the continuous release of microspheres and targeted delivery of nanocarriers to reasonably design a microsphere drug delivery system with a nanoparticle/micelle-microsphere double-layer structure, RANK siRNA and sCT were encapsulated by nanoparticles (AL-NPs) and ARM, respectively (Scheme S1 in Supporting information). Thereinto, nanoparticle was composed of AL coupled PLGA (AL-PLGA) and PEG-PLGA. AL has a high affinity for the main component of bone matrix of hydroxyapatite, which endows the nanoparticles with targeted delivery capability. ARM was composed of biocompatible material, egg phosphatidylcholine (Egg PC). Both of the two nanocarriers were encapsulated in Food and Drug Administration-approved PLGA/biocompatible material poly(cyclohexane-1,4-diylacetone dimethylene ketal) (PCADK) microspheres MS@(AL-NPs/ARM) as a drug delivery system, the double-layer structure protects biomacromolecules from rapid degradation, the outer microspheres can continuously release nanocarriers, and the released nanocarriers enter the blood circulation through the muscle vasculature to achieve bone targeted delivery [30]. Physicochemical properties of internal nanocarriers were characterized separately along with their effects on osteoblasts and osteoclasts. More importantly, the therapeutic advantages of size-switchable microspheres MS@(AL-NPs/ARM) were evaluated by comparison with conventional microspheres MS@(siRNA/sCT) through surface and internal morphology, *in vitro* release behavior, therapeutic effects within the glucocorticoid induced osteoporosis (GIOP) mouse model and on the regulation of relevant genes *in vivo* in mice.

We prepared a nanoscale drug delivery system for the targeted delivery of RANK siRNA for the treatment of osteoporosis (Fig. 1A). The particle size of AL-NPs was characterized using dynamic light scattering (DLS) and field emission scanning electron microscope (FESEM). AL-NPs exhibited an average diameter of 164.7 nm with a narrow size distribution (polydispersity index (PDI) = 0.102) as shown in Fig. 1C and Table S2 (Supporting information). The FE-SEM image of AL-NPs revealed the spherical shape with a surface morphology and size similar to that observed with DLS. RANK siRNA was efficiently encapsulated into AL-NPs with a high encapsulation efficiency (EE) of 87.3% (Table S2), and the effective loading of siRNA was visualized using agarose gel electrophoresis (Fig. S1 in Supporting information). The siRNA encapsulated in the nanoparticles remained in the loading well without migrating, whereas free siRNA moved downward due to the action of electric charge. Blank AL-NPs did not emit fluorescence either at the pore or at the position of free siRNA, whereas AL-NPs exhibited intense fluorescence only at the sample loading position, indicating successful encapsulation of siRNA into AL-NPs. The protective effect of AL-NPs on siRNA in the presence of nuclease was analyzed by agarose gel electrophoresis. As shown in Fig. 1E and Fig. S2 (Supporting information), AL-NPs could completely protect siRNA from nuclease degradation for at least 48 h, in contrast to naked siRNA. We simulated the release behavior of AL-NPs in PBS configured with DEPC-treated water, and the cumulative release of siRNA reached 63.1% within 72 h (Fig. S3 in Supporting information). Another nanocarrier was required to deliver sCT (Fig. 1B). Firstly, the half-life of sCT is as short as 0.5–1.0 h owing to the rapid clearance by macrophage, leading to low bioavailability [31]. Secondly, the physical and chemical instability of peptide drugs affects the drug loading capacity and limits microsphere fabrication [12]. We coated sCT with a unilamellar lipid vesicle by forming ARM to maintain its bioactivity and extend the mean residence time of sCT *in vivo*. The average particle size of ARM was approximately 268.0 nm with a narrow diameter distribution (PDI = 0.237) and the EE of ARM was about 59.7%. FESEM revealed a typical spherical structure of ARM with uniform particle size (Fig. 1D). The sCT release behavior of ARM was shown in Fig. 1F and the cumulative release was approximately 59.2% within 24 h. sCT was effectively released from the nanocarrier and bound to the receptor to achieve physiological effects.

PLGA-based biodegradable microspheres are promising drug carriers, that enable sustained release of medication over an extended period and protect fragile biomolecules from biodegradation, maintaining therapeutic levels of drugs for weeks to months with less frequent dosing. We designed a drug delivery system to encapsulate AL-NPs and ARM within PLGA/PCADK microspheres, aiming to achieve sustained release and dual protection of siRNA and sCT (Fig. 2A). The addition of PCADK could buffer acidic envi-

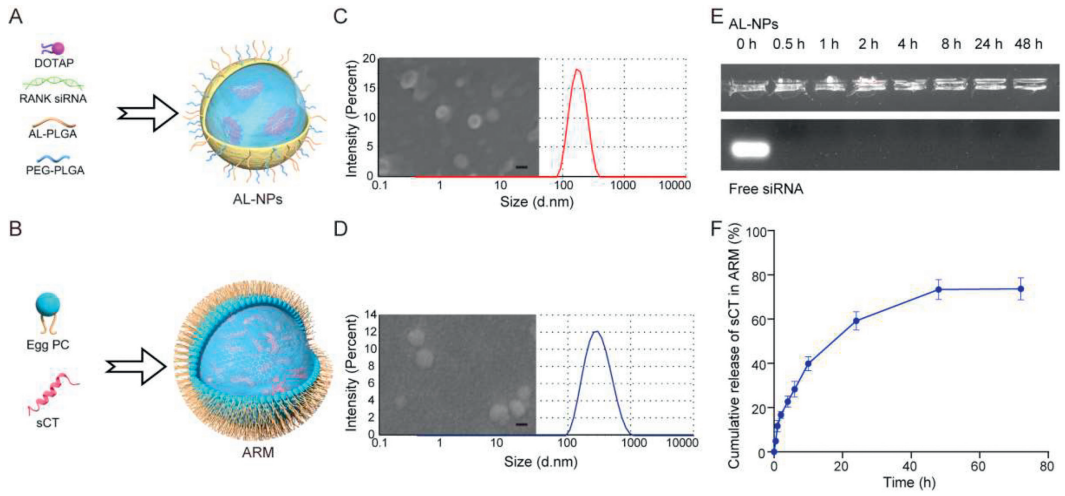


**Fig. 1.** The characterizations of AL-NPs and ARM. Schematic diagram of (A) AL-NPs and (B) ARM. (C) The size distribution and FESEM of AL-NPs. Scale bar: 150 nm. (D) The size distribution and FESEM of ARM. Scale bar: 150 nm. (E) Agarose gel electrophoresis analyzed the stability of siRNA loaded in AL-NPs. (F) *In vitro* cumulative release of sCT in ARM. Mean ± SEM ($n = 3$).

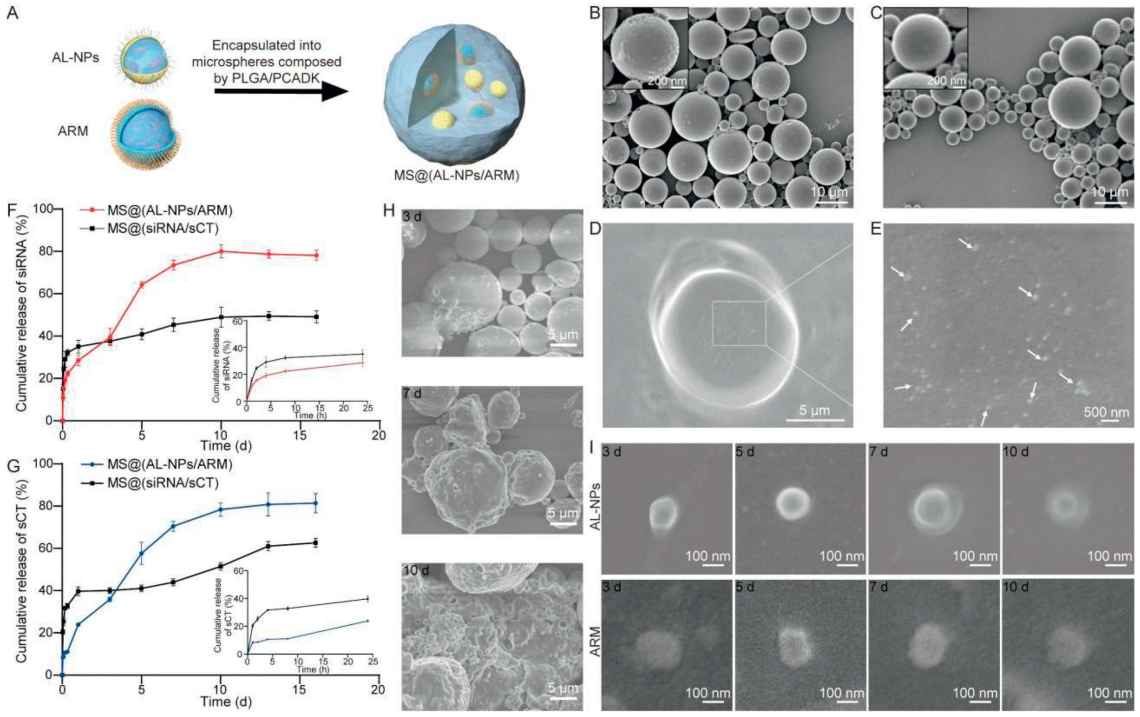


**Fig. 2.** Morphological characterization and *in vitro* release of MS@(AL-NPs/ARM) and MS@(siRNA/sCT). (A) Schematic diagram of MS@(AL-NPs/ARM). The FESEM of (B) MS@(AL-NPs/ARM) and (C) MS@(siRNA/sCT). Scale bar: 10 μm and 200 nm. (D) The FESEM of MS@(AL-NPs/ARM) by cryosections. Scale bar: 5 μm. (E) The FESEM of AL-NPs and ARM within MS@(AL-NPs/ARM). Scale bar: 500 nm. Release profiles of (F) siRNA and (G) sCT from MS@(AL-NPs/ARM) and MS@(siRNA/sCT) *in vitro* (Mean ± SEM, $n = 3$). (H) Morphological changes of MS@(AL-NPs/ARM) during *in vitro* release at 3, 7 and 10 d by FESEM. Scale bar: 5 μm. (I) The integrity verification of AL-NPs and ARM released from MS@(AL-NPs/ARM) detected by FESEM at 3, 5, 7 and 10 d. Scale bar: 100 nm.

ronment produced by PLGA degradation to maintain the stability of medication. The 20% PCADK was a rational ratio without causing rough surfaces and voids on the surface of the microspheres, as shown in Figs. 2B and C [32].

The dual-size microspheres of MS@(AL-NPs/ARM) improved the EE of siRNA and sCT from 19.8% ± 1.7% and 13.3% ± 3.0% to 53.6% ± 2.1% and 37.1% ± 1.1%, respectively, compared to that of MS@(siRNA/sCT) (Table S3 in Supporting information). The reason for this result may be that during the preparation of microspheres by w/o/w emulsion solvent evaporation method, for MS@(siRNA/sCT), siRNA and sCT in the internal aqueous phase were water-soluble. Due to the effect of osmotic pressure, drugs tended to penetrate into the external aqueous phase, leading to drugs leakage, while MS@(AL-NPs/ARM) could avoid this problem. The particle size and distribution of MS@(AL-NPs/ARM) and MS@(siRNA/sCT) were presented in Table S3 and Fig. S4 (Supporting information), respectively. The particle sizes of MS@(AL-NPs/ARM) and MS@(siRNA/sCT) were 14.6 ± 2.4 μm and 13.9 ± 1.9 μm, respectively, and there was little difference in the particle size distribution between the two kinds of microspheres. MS@(AL-NPs/ARM) were generally spherical with many small protrusions on the surface due to nanocarriers loading [33], while

MS@(siRNA/sCT) were typically depicted as a sphere encircled by a smooth surface (Figs. 2B and C). The dual-size microstructure of the microspheres was the basis of functional realization. Therefore, we sectioned MS@(AL-NPs/ARM) with cryosections to observe its interior. Many uniform nanoscale spheres dispersed inside the MS@(AL-NPs/ARM) (Figs. 2D and E). We speculated that the nanoscale spheres inside of MS@(AL-NPs/ARM) were AL-NPs and ARM due to similar particle size, shape and surface morphology to uncoated AL-NPs and ARM, respectively.

Cy5-siRNA and fluorescein isothiocyanate (FITC)-sCT were used to further investigate the co-location of fluorescence of nanocarriers in microspheres, to evaluate whether the two types of nanocarriers were co-loaded in the microspheres. The red and green fluorescence of Cy5-siRNA and FITC-sCT co-localized in the same microspheres, both MS@(AL-NPs/ARM) and MS@(siRNA/sCT) (Fig. S5 in Supporting information). The fluorescence intensity within MS@(AL-NPs/ARM) was uniformly distributed throughout the microspheres and higher than that of MS@(siRNA/sCT) considering EE. In contrast, the observed fluorescence intensity was mainly concentrated in the periphery of MS@(siRNA/sCT) because the siRNA and sCT solution in the internal water phase diffused outward during the preparation process [34], while AL-NPs and ARM as the less fluid inner water phase reduced the outward diffusion, resulting in difference in fluorescence distribution between MS@(siRNA/sCT) and MS@(AL-NPs/ARM). It could be inferred that the AL-NPs and ARM were uniformly encapsulated within the MS@(AL-NPs/ARM). The stability of microspheres was also an important index to evaluate the properties of microspheres, as shown in Table S4 (Supporting information), the microspheres could remain stable when stored at 4 °C for at least 14 days.

In drug delivery systems, *in vitro* release is considered as an important evaluation indicator of microspheres, with the requirement of low burst release and sustained, stable drug release [12]. We observed the release behavior of siRNA from MS@(AL-NPs/ARM) and MS@(siRNA/sCT) during 16 d as shown in Fig. 2F. MS@(siRNA/sCT) exhibited an obvious initial burst release, with 29.0% of siRNA being released from the microspheres within 4 h. This is a common phenomenon in polymer microspheres prepared by traditional emulsion solvent evaporation method, especially for highly hydrophilic drugs. The released siRNA from MS@(siRNA/sCT) already reached 35.0% within 1 d whereas a fast release plateau had been reached. The siRNA was gradually released, reaching 49.0% at the tenth day. In contrast, MS@(AL-NPs/ARM) effectively reduced the initial burst release of siRNA. The siRNA released from MS@(AL-NPs/ARM) in 4 h was 19.0% and the drug released on the first day was approximately 28.5%, lasting for 16 d. The cumulative siRNA release was approximately 78.0% from MS@(AL-NPs/ARM) at trial termination of 16 d.

Similarly, the release behavior of sCT from MS@(AL-NPs/ARM) and MS@(siRNA/sCT) was exhibited in Fig. 2G. Obvious burst release (20.5%) of sCT from MS@(siRNA/sCT) was observed within 1 h and the cumulative sCT release was approximately 62.6% during 16 d. For MS@(AL-NPs/ARM), the cumulative sCT release within 1 h was only 8.4%, representing a nearly three-fold decrease compared to MS@(siRNA/sCT), and the cumulative sCT release was 81.4% during 16 d, about 20% higher than that of MS@(siRNA/sCT). The difference in release between MS@(AL-NPs/ARM) and MS@(siRNA/sCT) maybe induced by the inconsistent distribution of free drugs and nanocarriers in microspheres (Fig. S5), the free siRNA and sCT in MS@(siRNA/sCT) were dispersed on the surface of the microspheres, resulting in fast release. siRNA and sCT in MS@(AL-NPs/ARM) were wrapped in AL-NPs and ARM, evenly distributed throughout MS@(AL-NPs/ARM) with a sustained release. Dual-size microspheres could control release the hydrophilic drugs by reducing initial burst release, extending release time and reduce the potential risk of drug overdose and subsequent insufficient drug release, comparing to conventional microspheres.

The morphology of dual-size microspheres during the release process was observed by FESEM (Fig. 2H). On the third day, the dissolution of MS@(AL-NPs/ARM) was observed with nanocarriers emergence, although the shape of microspheres remained relatively spherical. After centrifuging the microspheres, all the supernatants were removed, and fresh release medium was added. The corrosion and mutual fusion of MS@(AL-NPs/ARM) were observed on the seventh day, and the AL-NPs and ARM were found in the formed pores. MS@(AL-NPs/ARM) appeared swollen and deformed, tending to collapse on the tenth day. Furthermore, the integrity of nanocarriers is essential for achieving the intended physiological function. AL-NPs and ARM released from MS@(AL-NPs/ARM) will carry drugs into the blood circulation to reach the target site only when they maintain acceptable integrity. The integrity of the AL-NPs and ARM released from MS@(AL-NPs/ARM) was verified through direct observation by FESEM, and the structural changes in the nanocarriers in the supernatant were observed using FESEM over 10 days (Fig. 2I). We could more intuitively observe the spherical nanocarriers all through maintain integrity. The results indicated that AL-NPs/ARM released from MS@(AL-NPs/ARM) maintained the complete nano-structure, which facilitates the specific cellular uptake of AL-NPs and controlled release of sCT.

The effectiveness of RANK siRNA and sCT to inhibit osteoclast differentiation and activity was examined (Fig. S6 in Supporting information). Results showed that among all groups, the number of osteoclasts in the AL-NPs/ARM group was the lowest, which was not only because AL-NPs were easily taken up by cells to inhibit the differentiation of precursor cells into osteoclasts, but also because sCT in ARM could bind directly to CTR on osteoclasts to inhibit the activity of osteoclasts and induce their apoptosis. The mechanism of drug action was further explored by effects of RANK siRNA and sCT on the mRNA expression of osteoclasts and osteoblasts (Fig. S7 in Supporting information). The results showed that compared with siRNA, the expression of osteoclast related genes in the AL-NPs group was reduced to a greater extent. In addition, sCT upregulated the expression of osteoblast-related genes, while inhibiting the expression of RANKL to further inhibit the activity of osteoclasts (cell-related experimental results were discussed in detail in the Supporting information). These results provide a basis for the combination of AL-NPs and ARM for the treatment of osteoporosis.

Free siRNA, free sCT, NPs, AL-NPs and ARM with Cy5 fluorescent labeling were injected into GIOP mice *via* the caudal vein to evaluate the bone target and biodistribution of drugs. All animal experiments were approved by the Institutional Animal Ethics Committee of Jilin University (No. SY202111005). The fluorescence signals in various organs (heart, liver, spleen, lung, kidney) and legs of mice were observed at 4 h and 48 h (Figs. 3A–C). Firstly, under the same setting parameters, no fluorescence was observed in the organs and legs of GIOP mice without drug administration (Fig. S8 in Supporting information), indicating that the lesions of GIOP mice did not produce fluorescence to interfere with the accuracy of the experimental results. At 4 h, the total fluorescence of free siRNA was the lowest due to the barrier of uptake and circulation, which no obvious signal was shown in major organs except liver; The total fluorescence was the strongest in the AL-NPs group and fluorescence was highly accumulated in bone. At both 4 h and 48 h, the cumulative amount of sCT released from ARM was greater than that of free sCT in the bone, especially at 48 h the fluorescence intensity of ARM group was about 1.5 times that of the free sCT group. However, all the fluorescence accumulated in the legs at 48 h was very low. Therefore, microspheres controlled the continuous and stable release of nanocarriers contributes to the long-term treatment process. MS@(AL-NPs@Cy5-

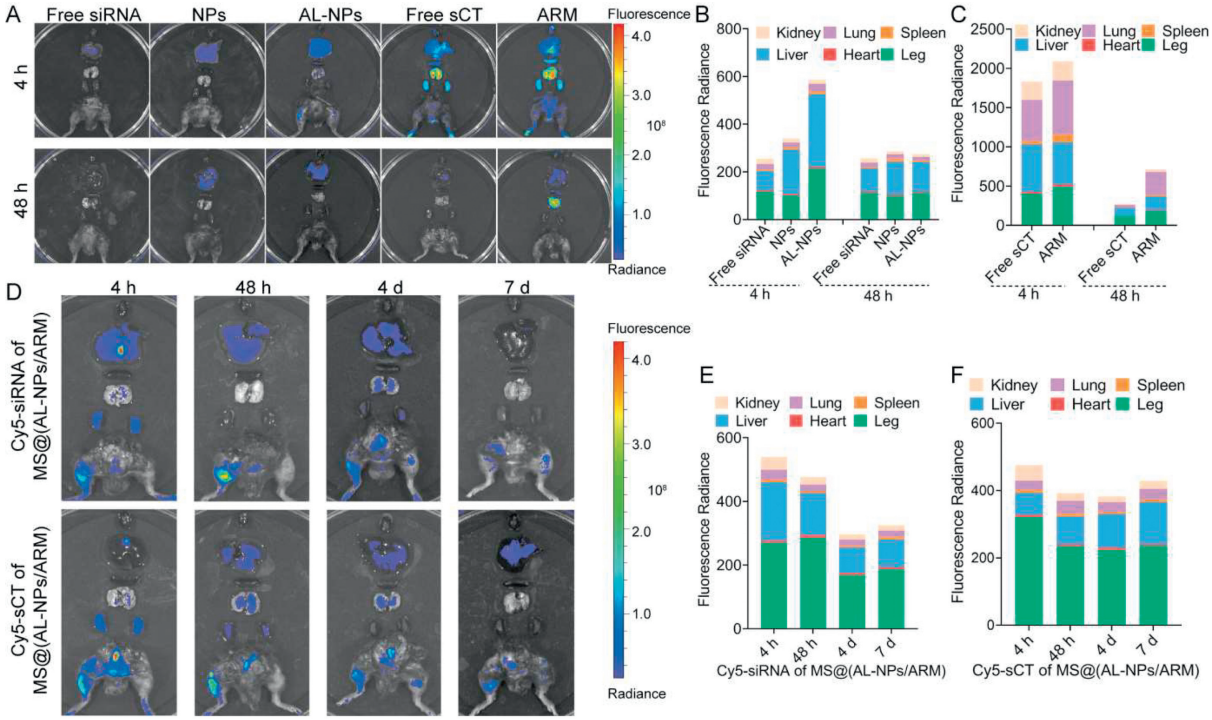


**Fig. 3.** Biodistribution of Cy5-siRNA and Cy5-sCT *in vivo*. (A) Biodistribution of Cy5-siRNA in AL-NPs and Cy5-sCT in ARM *in vivo* at 4 h and 48 h. The quantification of (B) Cy5-siRNA in AL-NPs and (C) Cy5-sCT in ARM *in vivo* at 4 h and 48 h. (D) Biodistribution of Cy5-siRNA and Cy5-sCT in MS@(AL-NPs/ARM) at 4 h, 48 h, 4 d and 7 d. The quantification of (E) Cy5-siRNA and (F) Cy5-sCT in MS@(AL-NPs/ARM) at 4 h, 48 h, 4 d and 7 d.

siRNA/ARM) and MS@(AL-NPs/ARM@Cy5-sCT) were injected into GIOP mice *via* muscle to assess the biodistribution and cumulative time of drugs in MS@(AL-NPs/ARM) at 4 h, 48 h, 4 d and 7 d. As shown in Figs. 3D–F, the fluorescence signal of either Cy5-siRNA or Cy5-sCT was still observed in the mice until the seventh day, indicating that MS@(AL-NPs/ARM) could effectively release drugs and prolong the circulation time of drugs *in vivo*. Importantly, fluorescent signal was observed for MS@(AL-NPs@Cy5-siRNA/ARM) in the contralateral part of the intramuscular injection site of femur and vertebrae within seven days, suggesting that AL-NPs released from the microspheres still retained the targeting ability to enrich the bone tissue site.

GIOP mice model was built to evaluate the therapeutic effect [35]. The principle of GIOP mice model was based on the long-term administration of glucocorticoids, such as dexamethasone, which promoted the expression of RANKL in cells, and in turn promoted the expression of reactive oxygen species (ROS). ROS could inhibit the activity of osteoblasts and activate the activity of osteoclasts, resulting in osteoporosis [36–40]. Free siRNA, free sCT, AL-NPs and ARM were administered by the caudal vein every three days for a total of five times, while MS@(AL-NPs/ARM) and MS@(siRNA/sCT) were administered as a single-dose treatment by the intramuscular injection (Fig. 4A) to maintain consistent total dosage. GIOP mice group exhibited thinner cortical bone and sparser trabecular bone in the femur and tibia (Figs. S9 and S10 in Supporting information) compared to healthy mice, indicating the successful establishment of GIOP models. The anti-osteoporotic effects of all drugs were demonstrated through Micro-CT reconstruction of the femur from a three-dimensional (3D) perspective and cross section (Fig. 4B). Compared to healthy mice, the mice in the GIOP group exhibited sparse cortical bone and cavities inside the cortical bone from a 3D perspective. Moreover, from the transverse section of the femur, the white cortical bone in the outer ring was very thin, and the yellow trabecular bone in the inner was also less and thinner. The GIOP condition in mice improved after undergoing various treatment strategies involving siRNA and/or sCT. Free drugs did not significantly improve osteoporosis, the number of femoral trabecular increased after free drugs were coated by AL-NPs or ARM. Compared to the monotherapy groups, the AL-NPs/ARM group showed an increase in cortical bone thickness and trabecular number. Importantly, the MS@(AL-NPs/ARM) group exhibited the best therapeutic effect in reconstructing the trabecular. Compared to MS@(siRNA/sCT), the 3D perspective of MS@(AL-NPs/ARM) showed fewer cavities in cortical bone and the reconstruction of cross section exhibited the significant increase in trabecular and the thickening of cortical bone, which was attributed to the fact that drugs released from MS@(siRNA/sCT) were naked and easily degraded, and the nanocarrier released from MS@(AL-NPs/ARM) provided good protection for the drugs. These results showed that dual-size microspheres can reduce the frequency of drugs administration while providing a better treatment effect on osteoporosis.

In addition, the microarchitectural parameters of the femur, such as cortical bone thickness (Ct.Th), trabecular thickness (Tb.Th), trabecular separation (Tb.Sp), bone mineral density (BMD) and bone volume/tissue volume (BV/TV) were measured to further estimate the bone strength (Figs. 4C–G). Ct.Th reflects the thickness and separation of cortical bone; Tb.Th and Tb.Sp reflect the thickness and separation of trabecular; BMD refers to the amount of mineral density in bone tissue and can be used to assess the risk of fracture; BV/TV reflects the changes in bone mass and can be used to evaluate the strength of trabecular bone [41–43]. Ct.Th, Tb.Th, BV/TV and BMD decreased in GIOP mice, while Tb.Sp increased. In contrast, Ct.Th, Tb.Th, BV/TV and BMD of MS@(AL-NPs/ARM) mice were higher than those of AL-NPs/ARM (11.9%, 6.0%, 24.4% and 2.0%) and MS@(siRNA/sCT) (12.4%, 7.8%, 19.6% and 2.9%), respectively. Meanwhile, Tb.Sp was decreased than AL-NPs/ARM (8.7%) and MS@(siRNA/sCT) (14.9%). The microarchitectural parameters of the femur were consistent with the 3D perspective and cross-section Micro-CT reconstruction of

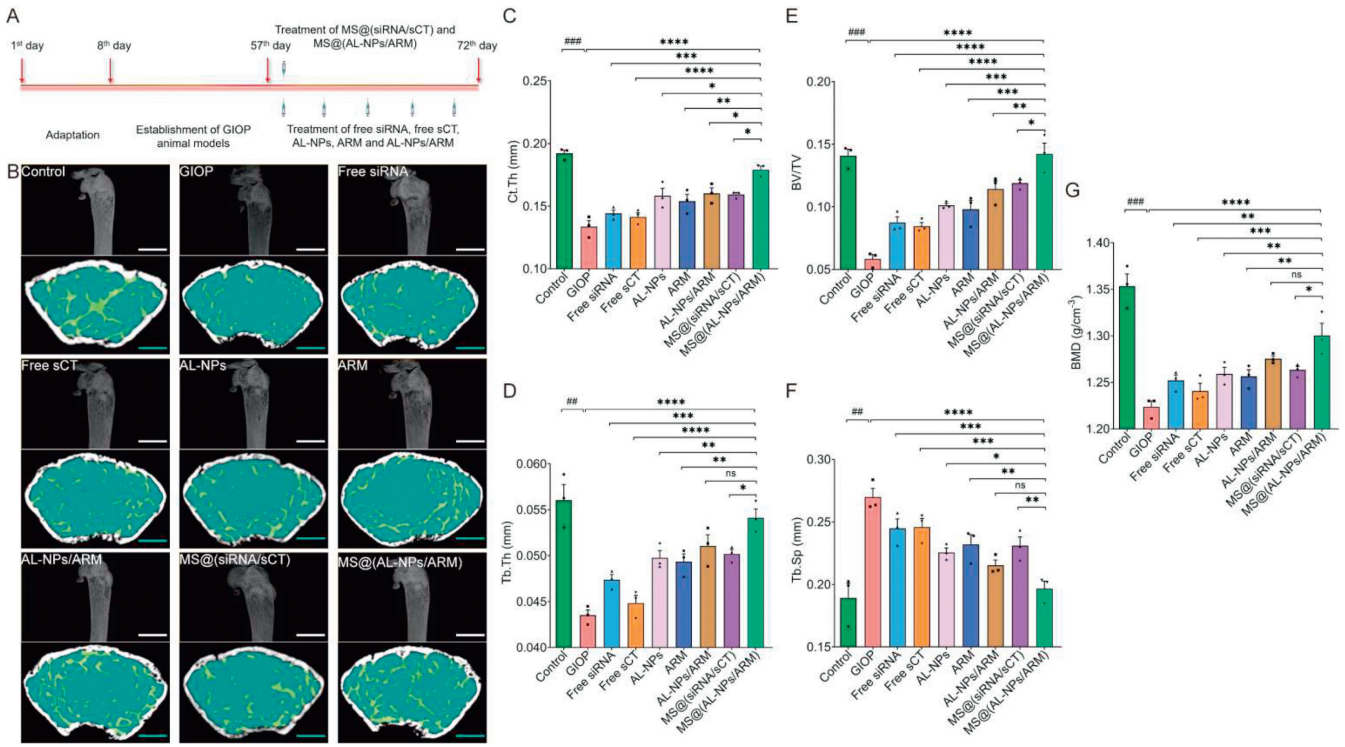


**Fig. 4.** Femoral scans and analysis of GIOP mice by Micro-CT. (A) Schematic diagram of GIOP mice model building and treatment. (B) 3D perspective and cross section of femur measured by Micro-CT at the endpoint of therapy (The white scale bar: 2 mm and the blue scale bar: 500 μm). The quantitative characterization of femur index by Micro-CT, including (C) Ct.Th, (D) Tb.Th, (E) BV/TV, (F) Tb.Sp and (G) BMD, respectively. Mean ± SEM ($n = 3$). $^{\#\#}P < 0.01$, $^{\#\#\#}P < 0.001$ *vs.* control mice; $^{*}P < 0.05$, $^{**}P < 0.01$, $^{***}P < 0.001$, $^{****}P < 0.0001$ *vs.* MS@(AL-NPs/ARM) mice. ns, no significance.

the femur, demonstrating that the dual-size microspheres had the most effective therapeutic outcome.

Through histological staining of the femurs of mice, it was visually demonstrated that MS@(AL-NPs/ARM) had the best therapeutic effect, and there was no abnormality in the visceral sections of mice, indicating the safety of using MS@(AL-NPs/ARM) (Figs. S11–S14 in Supporting information). In addition, in order to comprehend the mechanism of drug action in GIOP mice, the expression levels of osteoclast and osteoblast-related genes in leg bones were detected (Fig. S15 in Supporting information). The results showed that MS@(AL-NPs/ARM) exerted the best therapeutic effect by inhibiting osteoclasts and promoting osteoblasts. The detailed discussion of these three parts was in Supporting information.

In summary, this study successfully constructed size-switchable microsphere drugs delivery system co-loaded RANK siRNA and sCT to treat osteoporosis. The combination of RANK siRNA and sCT in MS@(AL-NPs/ARM) improved the therapeutic effect. In addition, the size-switchable microsphere system can achieve the sustained release of AL-NPs and ARM, which can protect drugs and deliver them to bone tissue to play a role, so as to reduce the frequency of administration and achieve long-term treatment. RANK siRNA and sCT co-delivery system based on the size-switchable microsphere is a potential carrier for delivering drugs to improve osteoporosis.

## Declaration of competing interest

The authors declare that they have no known competing financial interests or personal relationships that could have appeared to influence the work reported in this paper.

## Acknowledgments

The authors acknowledge the Central Lab of General Biology, Jilin University, China and Key Laboratory of Pathobiology, Ministry of Education, Jilin University, China for providing the research facilities to the team. This research was supported by the National Natural Science Foundation of China (Nos. 82003687, 52203138). This work was supported by the Jilin Scientific and Technological Development Program (No. 20200201415JC). This work was supported by the Finance Project of Jilin Province, China (Nos. 2019SRCJ016, 2020SCZT036). The authors would like to express our gratitude to Professor Youxin Li for his guidance.

## Supplementary materials

Supplementary material associated with this article can be found, in the online version, at doi:10.1016/j.cclet.2024.109668.

## References

[1] J.E. Compston, M.R. McClung, W.D. Leslie, Lancet 393 (2019) 364–376.
[2] X. Hao, X. Zhang, Y. Hu, et al., Chin. Chem. Lett. 34 (2023) 107965.
[3] S.S. Song, Y.Y. Guo, Y.H. Yang, D.H. Fu, Pharmacol. Ther. 237 (2022) 108168.
[4] T. Chen, D. Xiao, Y. Li, et al., Chin. Chem. Lett. 33 (2022) 2517–2521.
[5] D.M. Black, C.J. Rosen, N. Engl. J. Med. 374 (2016) 254–262.
[6] D.C. Bauer, Ann. Intern. Med. 171 (2019) JC22.
[7] C.H. Cheng, L.R. Chen, K.H. Chen, Int. J. Mol. Sci. 23 (2022) 1376.
[8] R. Sun, J. Song, S.J. Liu, et al., Chin. Chem. Lett. 22 (2011) 256–259.
[9] D.K. Khajuria, R. Razdan, D.R. Mahapatra, Rev. Bras. Reumatol. 51 (2011) 365–382.
[10] X. Sun, J. Wei, J. Lyu, et al., J. Nanobiotechnol. 17 (2019) 10.
[11] S.L. Ruggiero, T.B. Dodson, L.A. Assael, et al., Aust. Endod. J. 35 (2009) 119–130.
[12] S. Cao, Y. Liu, H. Shang, et al., J. Control. Release 256 (2017) 182–192.
[13] W.C. Dougall, M. Glaccum, K. Charrier, et al., Genes Dev. 13 (1999) 2412–2424.
[14] J. Jules, J.W. Ashley, X. Feng, Expert Opin. Ther. Targets 14 (2010) 923–934.
[15] N.A.T. Hamdy, Curr. Osteoporos. Rep. 3 (2005) 121–125.
[16] Y. Wang, K.K. Tran, H. Shen, D.W. Grainger, Biomaterials 33 (2012) 8540–8547.
[17] Y.P. Liu, X.B. Chen, S.Y. Li, et al., ACS Appl. Mater. Inter. 9 (2017) 23428–23440.
[18] P.M. Mountziaris, D.C. Sing, S.A. Chew, et al., Pharm. Res. 28 (2011) 1370–1384.
[19] F. Hu, J. Qi, Y. Lu, H. He, W. Wu, Chin. Chem. Lett. 34 (2023) 108250.
[20] Z.W. Wang, M. Fu, Y.P. Wang, et al., ACS Biomater. Sci. Eng. 6 (2020) 485–493.
[21] M. Li, S.F. Li, J.H. Liu, et al., J. Biomed. Mater. Res. A 107 (2019) 1832–1840.
[22] J.E. Adair, M.D. Weitzman, Mol. Ther. 22 (2014) 1397–1398.

[23] M.A. Islam, E.K.G. Reesor, Y.J. Xu, et al., Biomater. Sci. 3 (2015) 1519–1533.
[24] L.F. Zhang, J.M. Chan, F.X. Gu, et al., ACS Nano 2 (2008) 1696–1702.
[25] D. Guo, X. Ji, F. Peng, et al., Nanomicro Lett. 11 (2019) 27.
[26] R. Liu, C. Luo, Z. Pang, et al., Chin. Chem. Lett. 34 (2023) 107518.
[27] L. Shang, T. Yang, C. Yang, et al., Chem. Eng. J. 425 (2021) 131420.
[28] X. Sun, S. Dong, X. Li, et al., Nanomedicine 20 (2019) 102017.
[29] M. Omidi, V. Mansouri, L.M. Amirabad, L. Tayebi, ACS Appl. Mater. Inter. 13 (2021) 24370–24384.
[30] Y. Li, R. Jarvis, K. Zhu, et al., Angew. Chem. Int. Ed. 59 (2020) 14957–14964.
[31] P. Yu, Y.P. Liu, R.T. Jin, et al., ACS Biomater. Sci. Eng. 6 (2020) 4077–4086.
[32] J. Liu, S. Li, G. Li, et al., Int. J. Pharm. 563 (2019) 228–236.
[33] H. Park, D.H. Ha, E.S. Ha, et al., Pharmaceutics 11 (2019) 627.
[34] Y.S. Lee, J.P. Lowe, E. Gilby, S. Perera, S.P. Rigby, Int. J. Pharm. 383 (2010) 244–254.
[35] A. Xavier, H. Toumi, E. Lespessailles, Int. J. Mol. Sci. 23 (2022) 377.
[36] Y. Chu, Y. Luo, B. Su, et al., Acta Pharm. Sin. B 13 (2023) 298–314.
[37] T. Sun, C. Jiang, Adv. Drug Deliv. Rev. 196 (2023) 114773.
[38] T. Sun, Q. Chen, Z. Zhou, et al., J. Control. Release 358 (2023) 382–397.
[39] J.S. Kimball, J.P. Johnson, D.A. Carlson, J. Bone Joint Surg. Am. 103 (2021) 1451–1461.
[40] M.M. Conradie, A.C.B. Cato, W.F. Ferris, et al., Calcif. Tissue Int. 89 (2011) 221–227.
[41] J. Wang, S. Tao, X. Jin, et al., Theranostics 10 (2020) 8591–8605.
[42] D. Huang, C. Zhao, R. Li, et al., Nat. Commun. 13 (2022) 5338.
[43] F. Yu, D. Geng, Z. Kuang, et al., Asian J. Pharm. 17 (2022) 425–434.